Physics of the Dark Universe 45 (2024) 101545

Contents lists available at ScienceDirect

Physics of the Dark Universe

journal homepage: www.elsevier.com/locate/dark

Full length article

Linear redshift parametrization of deceleration parameter in $f(R, L_m)$ gravity

Yerlan Myrzakulov [a,b,*], O. Donmez [c,**], G. Dilara A. Yildiz [d,e], E. Güdekli [f], S. Muminov [g], J. Rayimbaev [h,i,j]

[a] Department of General & Theoretical Physics, L.N. Gumilyov Eurasian National University, Astana, 010008, Kazakhstan
[b] Ratbay Myrzakulov Eurasian International Center for Theoretical Physics, Astana, 010009, Kazakhstan
[c] College of Engineering and Technology, American University of the Middle East, Egaila 54200, Kuwait
[d] Graduate School of Engineering and Science, Istanbul University, Istanbul 34134, Turkey
[e] Department of Physics, Faculty of Science and Letters, Piri Reis University, 34940 Tuzla, Istanbul, Turkey
[f] Department of Physics, Istanbul University, Istanbul 34134, Turkey
[g] Urgench State University, Kh. Alimjan str. 14, Urgench 221100, Uzbekistan
[h] New Uzbekistan University, Mustaqillik Ave. 54, Tashkent 100007, Uzbekistan
[i] University of Tashkent for Applied Sciences, Gavhar Str. 1, Tashkent 100149, Uzbekistan
[j] National University of Uzbekistan, Tashkent 100174, Uzbekistan

ARTICLE INFO

Keywords:
$f(R,L_m)$ gravity
Deceleration parameter
Observational constraints
Dark energy

ABSTRACT

In this study, we investigate the linear redshift parametrization of $q(z)$ within the framework of $f(R, L_m)$ gravity, using constraints derived from $H(z)/Pantheon$ samples. We consider a non-linear functional form for $f(R, L_m)$, specifically given by $f(R, L_m) = \frac{R}{2} + L_m^n$, where n represents a free parameter in the model. Subsequently, we derive the solution for the Hubble parameter by investigating the parametrization of $q(z)$ and then apply this solution to the modified Friedmann equations. Our analysis focuses on exploring the behavior of the EoS parameter across different stages of the universe's evolution, including radiation, matter, and dark energy eras. Furthermore, our results confirm the quintessence nature of the universe's current accelerated expansion phase ($-1 < \omega < -\frac{1}{3}$), supporting the role of quintessence in driving the universe's current acceleration. We also explore the redshift dependence of the deceleration parameter, statefinder, $Om(z)$ diagnostics, energy density, pressure, and energy conditions to determine the universe's accelerating behavior. Importantly, our findings suggest that the linear redshift parametrization of $q(z)$, supported by additional terms in $f(R, L_m)$ gravity, provides a compelling alternative to the cosmological constant.

1. Introduction

General Relativity (GR) is widely accepted as the prevailing theory of gravitation due to its successful validation through numerous experimental and observational tests. For instance, the recent detection of gravitational waves by the Virgo and LIGO detectors provides compelling evidence in support of GR's predictions [1–5]. While GR has demonstrated remarkable success, particularly in the context of gravitational wave detections, several theoretical challenges persist. These challenges have motivated researchers to seek modifications or alternatives to GR. For instance, GR does not offer sufficient explanations for certain issues, such as the initial singularity problem, flatness problems, fine-tuning, the cosmological constant problem, and the cosmic coincidence problem [6–9]. Addressing these challenges requires exploring theoretical frameworks beyond the scope of GR.

To address these challenges, various modified theories have been proposed in the scientific literature. These theories have been crucial in studying the behavior of the accelerating universe. Some modifications have been made to the gravitational part of the Einstein–Hilbert (EH) action, as explored in studies [10–24]. In addition, modifications to the matter part of the EH action have led to the development of dynamical models such as quintessence, Chaplygin gas, k-essence, and holographic dark energy (DE) models, as discussed in research [25–33]. These modified models have shown promise in effectively explaining the current accelerated expansion of the universe, as observed through various observational methods such as high-redshift Supernovae (SNe), the Cosmic Microwave Background Radiation (CMBR), the Wilkinson Microwave Anisotropy Probe (WMAP), Baryonic Acoustic Oscillations

* Corresponding author at: Department of General & Theoretical Physics, L.N. Gumilyov Eurasian National University, Astana, 010008, Kazakhstan.
** Corresponding author at: College of Engineering and Technology, American University of the Middle East, Egaila 54200, Kuwait.
E-mail addresses: ymyrzakulov@gmail.com (Y. Myrzakulov), orhan.donmez@aum.edu.kw (O. Donmez), gizemdilaraacan@gmail.com (G.D.A. Yildiz), gudekli@istanbul.edu.tr (E. Güdekli), sokhibjan.m@urdu.uz (S. Muminov), javlon@astrin.uz (J. Rayimbaev).

https://doi.org/10.1016/j.dark.2024.101545
Received 18 May 2024; Received in revised form 28 May 2024; Accepted 28 May 2024
Available online 31 May 2024

(BAOs), and studies of Large Scale Structure (LSS). These findings are documented in sources such as [34–42].

One of the simplest modified theories is known as $f(R)$ gravity, where the standard EH action of GR is altered by introducing a generic function $f(R)$, with R representing the Ricci scalar curvature [43–45]. The late-time expansion scenario can be described using $f(R)$ gravity [46], and constraints on viable cosmological models have been examined in [47,48]. Viable $f(R)$ gravity models that pass solar system tests do exist [49–52]. Observational signatures of $f(R)$ DE models, along with constraints from the solar system and equivalence principles on $f(R)$ gravity, have been investigated in [53–57]. Other $f(R)$ models that unify early inflation with DE and pass local tests have been discussed in [58–60]. For various cosmological implications of $f(R)$ gravity models, one can refer to [61–63].

An extension of the $f(R)$ gravity theory was proposed in [64], introducing an explicit coupling between the matter Lagrangian density L_m and the generic function $f(R)$. Due to this coupling between matter and geometry, a new force perpendicular to the four-velocity vector arises, leading to the non-geodesic motion of massive particles. This model was further developed to incorporate arbitrary couplings in both matter and geometry [65]. The cosmological and astrophysical consequences of the non-minimal matter–geometry couplings have been extensively studied in [66–70]. Harko and Lobo [71] recently introduced a more advanced version of matter–curvature coupling theories known as $f(R, L_m)$ gravity theory. In this theory, $f(R, L_m)$ denotes an arbitrary function of the matter Lagrangian density L_m and the Ricci scalar R. In the $f(R, L_m)$ gravity theory, which can be seen as the most comprehensive extension of gravitational theories formulated in the Riemannian manifold, the movement of test particles is non-geodesic, leading to the appearance of an additional force perpendicular to the four-velocity vector. The $f(R, L_m)$ gravity models allow for an explicit violation of the equivalence principle, a feature that is strongly constrained by solar system tests [72,73]. Wang and Liao conducted a study on energy conditions in $f(R, L_m)$ gravity [74], while Gonclaves and Moraes analyzed cosmological aspects considering the non-minimal matter–geometry coupling within the framework of $f(R, L_m)$ gravity [75]. Recently, there have been notable developments in the study of $f(R, L_m)$ gravity, as evidenced by several significant results [76–78].

In the presented manuscript, we investigate the cosmological $f(R, L_m)$ model, which encompasses both a deceleration and an accelerated phase of expansion. In this context, the parametrization of the deceleration parameter q is pivotal in describing the universe's expansion rate. Typically, the deceleration parameter is expressed as

$$q(z) = \alpha X(z) + \beta, \tag{1}$$

where α and β are arbitrary constants, and $X(z)$ is a function of redshift z. In the literature [79–85], various redshift functions $X(z)$ have been proposed. While some of these functions offer satisfactory solutions to cosmological problems such as the initial singularity problem, flatness problems, fine-tuning, and the cosmological constant problem, they may fail to accurately predict the future evolution of the universe. On the other hand, certain redshift functions are reliable only for small values of z, limiting their applicability to specific cosmological scenarios. In this study, we select the functional form $f(R, L_m) = \frac{R}{2} + L_m^n$ (where n is a model parameter) for several reasons. This choice is motivated by the need to introduce a simple yet effective modification to the standard Einstein–Hilbert action, allowing us to explore the effects of a non-linear matter term on cosmological dynamics. The term $\frac{R}{2}$ retains a connection to the Ricci scalar component in GR, ensuring that our model can reduce to GR under the condition where $n = 1$. Within this framework, we explore several cosmological implications, using the Hubble function $H(z)$ obtained directly from the linear redshift parametrization of $q(z)$ [80]. Our investigation focuses on analyzing various cosmological parameters within the context of a flat FLRW universe.

The current manuscript is structured as follows. Section 2 provides an overview of the action and fundamental formulation governing the dynamics within $f(R, L_m)$ gravity, along with the modified Friedmann equations relevant to the flat FLRW universe. In Section 3, we employ the linear redshift parametrization of $q(z)$ to derive the expression for the Hubble parameter $H(z)$. We then determine the model parameters that align with observational data by incorporating the $H(z)$, *Pantheon*, and the combined $H(z)$ + *Pantheon* analysis datasets. In addition, we analyze various geometrical parameters, including the deceleration parameter, statefinder, and $Om(z)$ diagnostics, to assess the DE behavior predicted by the assumed model. Section 4 is dedicated to investigating the energy density, pressure, EoS parameter, and energy conditions. Finally, in Section 5, we summarize our findings.

2. Exploring $f(R, L_m)$ gravity: A comprehensive review

The expression for the gravitational action in the $f(R, L_m)$ context is provided as follows [71]:

$$S = \int f(R, L_m)\sqrt{-g}d^4x. \tag{2}$$

Here, g denotes the metric determinant, and $f(R, L_m)$ is a versatile function encompassing both R (the Ricci scalar) and L_m (the matter Lagrangian) as its variables. In addition, we will employ natural units as our preferred system of measurement throughout this article.

By performing variations on the action (2) with respect to the metric tensor $g_{\mu\nu}$, we obtained the field equation that governs the dynamics of gravitational interactions,

$$f_R R_{\mu\nu} + (g_{\mu\nu}\Box - \nabla_\mu\nabla_\nu)f_R - \frac{1}{2}(f - f_{L_m}L_m)g_{\mu\nu} = \frac{1}{2}f_{L_m}T_{\mu\nu}. \tag{3}$$

Here, we introduce the notations $f_R \equiv \frac{\partial f}{\partial R}$ and $f_{L_m} \equiv \frac{\partial f}{\partial L_m}$. Furthermore, $T_{\mu\nu}$ represents the energy–momentum tensor for a perfect fluid, as defined by

$$T_{\mu\nu} = \frac{-2}{\sqrt{-g}}\frac{\delta(\sqrt{-g}L_m)}{\delta g^{\mu\nu}}. \tag{4}$$

Moreover, upon computing the covariant derivative of Eq. (3), we arrive at the following outcome:

$$\nabla^\mu T_{\mu\nu} = 2\nabla^\mu ln(f_{L_m})\frac{\partial L_m}{\partial g^{\mu\nu}}. \tag{5}$$

To explore the cosmological implications, we delve into the considerations of a homogeneous and spatially isotropic flat Friedmann–Lemaître–Robertson–Walker (FLRW) metric. This metric provides a suitable framework for investigating the large-scale structure and evolution of the universe [86],

$$ds^2 = -dt^2 + a^2(t)[dx^2 + dy^2 + dz^2], \tag{6}$$

where $a(t)$ is the scale factor governing the expansion of the universe at a given time t. Now, by using the line element (6), we calculated the Ricci scalar as,

$$R = 6(\dot{H} + 2H^2), \tag{7}$$

where $H = \frac{\dot{a}}{a}$ represents the Hubble parameter, with $\dot{a}$ denoting the time derivative of the scale factor a, the Hubble parameter characterizes the rate at which the universe is expanding.

The energy–momentum tensor, which includes the energy density ρ and the spatially isotropic pressure p of the cosmic fluid without viscosity effects, is expressed as

$$\mathcal{T}_{\mu\nu} = (\rho + p)u_\mu u_\nu + pg_{\mu\nu}, \tag{8}$$

where $u^\mu = (1, 0, 0, 0)$ denotes the components of the 4-velocity vector for the cosmic fluid.

The Friedmann equations, elucidating the dynamics of the Universe within the framework of $f(R, L_m)$ gravity, can be succinctly expressed as [76],

$$3H^2 f_R + \frac{1}{2}\left(f - f_R R - f_{L_m} L_m\right) + 3H\dot{f}_R = \frac{1}{2} f_{L_m}\rho, \tag{9}$$

and

$$\dot{H} f_R + 3H^2 f_R - \ddot{f}_R - 3H\dot{f}_R + \frac{1}{2}\left(f_{L_m} L_m - f\right) = \frac{1}{2} f_{L_m} p. \tag{10}$$

To investigate the behavior of the universe, we explore the following functional form within the context of the $f(R, L_m)$ cosmological model [76–78],

$$f(R, L_m) = \frac{R}{2} + L_m^n, \tag{11}$$

where n represents the model's free parameter. Notably, when $n = 1$, the equations revert to the standard Friedmann equations of GR. In the case of the specific $f(R, L_m)$ model under consideration, where $L_m = \rho$ [87,88], the Friedmann Eqs. (9) and (10) can be written as,

$$3H^2 = (2n-1)\rho^n, \tag{12}$$

$$2\dot{H} + 3H^2 = [(n-1)\rho - np]\,\rho^{n-1}. \tag{13}$$

The system of Eqs. (12) and (13) described above contains only two independent equations with three unknowns: ρ, p, and H. To find exact solutions, an additional constraint must be added. This is often achieved by assuming the dust matter ($p = 0$) [76] or using parametrization techniques [77,78]. One such technique is the parametrization of geometrical parameters such as the Hubble parameter, jerk parameter, and deceleration parameter, which provides the redshift dependence of all cosmological parameters. Another approach is the parametrization of the physical parameters, such as the energy density, pressure, and equation of state, which also gives the redshift dependence of all cosmological parameters. This method is commonly known as a model-independent way to study cosmological models [89, 90]. In the next section, we will delve into the study of $f(R, L_m)$ gravity within the framework of the linear redshift parametrization of the deceleration parameter $q(z)$.

3. Linear redshift parametrization of $q(z)$

The extensive cosmological observations provide compelling evidence that the expansion of the universe has shifted from a decelerating phase, where the cosmic expansion was slowing down, to an accelerating one, indicating an increase in the rate of expansion. This transformative shift in the dynamics of the universe has significant implications for our understanding of its evolution and the underlying forces driving these changes. For these reasons, we assume the linear redshift parametrization form of $q(z)$, as detailed below [80]:

$$q(z) = \alpha z + \beta, \tag{14}$$

where α represents the linear slope coefficient, providing insights into the rate of change of $q(z)$ with redshift, while the constant term $\beta = q_0$ captures the present-day value of $q(z)$ (i.e. at $z = 0$). It is noteworthy that the chosen parametric form for $q(z)$ draws inspiration from a well-established linear parametrization commonly used for the DE equation of state i.e. $\omega(z) = \omega_1 z + \omega_0$ [91]. This choice demonstrates its versatility and adaptability, proving effective in capturing the $q(z)$ behavior exhibited by a broad range of accelerating models. Furthermore, the linear parametrization has been widely used and validated in previous studies [79–85], demonstrating its robustness in fitting observational data. It provides a good first-order approximation that is sufficient for our analysis, given the current level of precision in observational datasets.

The equation establishes a relationship between the deceleration parameter and the Hubble parameter, represented as,

$$H(z) = H_0 \exp\left(\int_0^z \frac{1+q(z)}{(1+z)} dz\right). \tag{15}$$

By inserting the expression from Eq. (14) into Eq. (15), we derive the formula for $H(z)$ as,

$$H(z) = H_0 e^{\alpha z}(1+z)^{-\alpha+\beta+1}, \tag{16}$$

where H_0 denotes the present value of the Hubble parameter at $z = 0$. The time derivative of the Hubble parameter can be expressed as,

$$\dot{H} = \frac{dH}{dt} = -(1+z)\,H(z)\,\frac{dH(z)}{dz}. \tag{17}$$

For the linear redshift parametrization of $q(z)$, Eq. (17) becomes,

$$\dot{H} = -H_0^2 e^{2\alpha z}(\alpha z + \beta + 1)(1+z)^{-2\alpha+2\beta+2}. \tag{18}$$

In the upcoming subsection, our focus is on ensuring the model's reliability and adherence to the most recent observations. To achieve this, we constrain the model's parameters (H_0, α, β) by leveraging information from two contemporary observational datasets, namely, the Hubble $H(z)$ dataset and the Pantheon dataset.

3.1. Observational data

In our study, we use two primary datasets: the $H(z)$ dataset and the Pantheon dataset. The $H(z)$ dataset consists of measurements of the Hubble parameter at various redshifts, which provide direct information about the expansion rate of the universe. The Pantheon dataset includes a compilation of Type Ia Supernovae (SNe Ia) observations, offering constraints on the distance modulus across a range of redshifts. To integrate these datasets into our analysis, we follow these steps:

1. **Modeling the Hubble parameter** $H(z)$: We employ the linear redshift parametrization of the deceleration parameter $q(z)$ to derive the expression for the Hubble parameter $H(z)$. The resulting functional form is provided in Eq. (16).
2. **Combined Likelihood function**: For both the $H(z)$ and Pantheon datasets, we construct the likelihood functions. To obtain the best-fit values for the model parameters, we then combine the likelihoods from both datasets: $\mathcal{L}_{\text{total}} = \mathcal{L}_{H(z)} \times \mathcal{L}_{\text{Pantheon}}$. Here, $\mathcal{L} = \exp(-\chi^2/2)$, where χ^2 denotes the chi-squared function [92]. The specific forms of the χ^2 functions used for different datasets are provided below.
3. **Parameter estimation**: We use Markov Chain Monte Carlo (MCMC) methods facilitated by the Python library [93] to sample the parameter space and estimate the best-fit values and their uncertainties. The MCMC approach provides a robust framework for exploring the multi-dimensional parameter space and obtaining the posterior distributions of the parameters α, β, and H_0.
4. **Statistical significance**: The statistical significance of the best-fit values is assessed using the credible intervals derived from the posterior distributions. We report the median values along with the 68% confidence intervals for each parameter. In addition, we evaluate the goodness-of-fit using the chi-square statistic and compare the model predictions with the observational data.

3.1.1. $H(z)$ Dataset

We utilize a dataset comprising 31 data points obtained via the Cosmic Chronometers (CC) technique. This method enables us to directly derive information about the Hubble parameter $H(z)$ at various redshifts, extending up to $z \leq 2$. The decision to use CC data is primarily based on its reliance on age difference measurements between two passively evolving galaxies. These galaxies originated simultaneously but are separated by a small redshift interval. This approach enables the calculation of $\Delta z/\Delta t$. It is worth noting that CC data has shown greater reliability compared to other methods that depend on absolute age determinations for galaxies [94]. The CC data points used in our analysis were collected from independent sources referenced in [95–101]. These sources are not reliant on the Cepheid distance scale or any specific cosmological model. However, it is important to recognize

Table 1
A summary is provided, detailing the best-fit values of model parameters and statistical analysis using $H(z)$, *Pantheon*, and $H(z)+$*Pantheon* datasets, along with the 68% and 95% confidence levels.

Datasets	H_0 (km/s/Mpc)	α	$\beta = q_0$	z_{tr}	ω_0
Priors	(60, 80)	(−1, 1)	(−1, 1)	–	–
$H(z)$	$67.7^{+1.7}_{-1.7}$	$0.54^{+0.42}_{-0.43}$	$-0.40^{+0.24}_{-0.24}$	$0.74^{+0.57}_{-0.58}$	$-0.49^{+0.09}_{-0.09}$
Pantheon	$67.8^{+2.8}_{-2.9}$	$0.58^{+0.43}_{-0.62}$	$-0.45^{+0.30}_{-0.27}$	$0.78^{+0.63}_{-0.63}$	$-0.61^{+0.22}_{-0.20}$
$H(z)+$*Pantheon*	$67.8^{+1.5}_{-1.5}$	$0.65^{+0.33}_{-0.32}$	$-0.46^{+0.18}_{-0.17}$	$0.71^{+0.42}_{-0.41}$	$-0.61^{+0.12}_{-0.12}$

that these data points depend on the modeling of stellar ages, which is grounded in robust techniques of stellar population synthesis. For further details on the analyses related to CC systematics, refer to Refs. [97,99,102–105]. The assessment of the model's performance in fitting this dataset involves the computation of the χ^2 function, defined as,

$$\chi^2_{H(z)}(H_0,\alpha,\beta) = \sum_{i=1}^{31} \frac{\left[H(z_i,H_0,\alpha,\beta) - H_{obs}(z_i)\right]^2}{\sigma^2(z_i)}. \tag{19}$$

Here, H_{obs} signifies the observed value, while $\sigma(z_i)$ represents the observational error corresponding to each data point.

3.1.2. Pantheon dataset

Given their role as standard candles offering robust estimates of cosmic distances, SNe Ia plays a crucial role in constraining the DE sector. In our investigation, we rely on the Pantheon compilation, encompassing 1048 data points distributed within the redshift range of $0.01 < z < 2.26$ [106]. The χ^2 function associated with this dataset is articulated as,

$$\chi^2_{Pantheon}(H_0,\alpha,\beta) = \sum_{i=1}^{1048} \frac{\left[\mu(H_0,\alpha,\beta,z_i) - \mu_{obs}(z_i)\right]^2}{\sigma^2(z_i)}. \tag{20}$$

Here, μ_{obs} denotes the observational distance modulus, and $\sigma(z_i)$ represents the observational error associated with each data point. In addition, we define $\mu = m_B - M_B$, where m_B represents the observed apparent magnitude at a given redshift and M_B is the absolute magnitude. The determination of nuisance parameters is carried out using the BBC approach [107].

The theoretical distance modulus $\mu(z)$ is a fundamental component in our analysis, representing the predicted measure of the cosmic distance at a given redshift. It is defined as,

$$\mu(z) = 5log_{10}\left[\frac{d_L(z)}{1Mpc}\right] + 25. \tag{21}$$

Here, $d_L(z)$ represents the luminosity distance and is defined as,

$$d_L(z) = \frac{c(1+z)}{H_0} S_k\left(H_0\int_0^z \frac{1}{H(y,H_0,\alpha,\beta)}dy\right),$$

$$\text{where } S_k(x) = \begin{cases} \sinh(x\sqrt{\Omega_k})/\Omega_k, & \Omega_k > 0 \\ x, & \Omega_k = 0 \\ \sin(x\sqrt{|\Omega_k|})/|\Omega_k|, & \Omega_k < 0 \end{cases}$$

In the context of a flat universe, we obtain

$$d_L(z) = c(1+z)\int_0^z \frac{dy}{H(y,H_0,\alpha,\beta)}, \tag{22}$$

where c denotes the speed of light.

The constraints on the model parameters are determined by minimizing the corresponding χ^2 using the MCMC approach. The outcomes of this analysis are presented in Table 1. Furthermore, in Fig. 1, an error bar fit for the considered model is juxtaposed with the ΛCDM model characterized by $\Omega_{m0} = 0.315$ and $H_0 = 67.4$ km/s/Mpc [108]. To visually represent the constraints, contour plots depicting the 1-σ and 2-σ confidence levels are presented for the $H(z)$, *Pantheon*, and the joint observational datasets in Figs. 2, 3, and 4, respectively.

3.2. Deceleration parameter

The dimensionless representation of the second-order time derivative of the scale factor i.e. $q = -1 - \frac{\dot{H}}{H^2}$, known as the deceleration parameter, is illustrated in Fig. 5. Within the proposed model, the deceleration parameter exhibits a distinctive transition, ranging from 0.70 to 0.80, consistent with findings in previous studies [109–112]. As a pivotal indicator of the universe's dynamic behavior, the deceleration parameter serves to discern whether the cosmic expansion is accelerating or decelerating. Specifically, a positive q implies a decelerating expansion, $q = 0$ corresponds to a constant rate of expansion, and acceleration is indicated when $-1 < q < 0$. In addition, the universe demonstrates exponential expansion or de Sitter expansion for $q = -1$, while super-exponential expansion occurs for $q < -1$. Table 1 displays the current value of the deceleration parameter associated with the model parameters constrained by the $H(z)$, *Pantheon*, and $H(z)+$*Pantheon* datasets [113–120]. The results distinctly reveal the late-time cosmic acceleration of the universe and the deceleration expansion in the past.

3.3. Statefinder diagnostic

The role of DE in driving cosmic expansion is widely acknowledged. Over the past few decades, there has been a surge in investigations aiming to understand the origin and fundamental characteristics of DE. As a result, numerous DE models have emerged, necessitating a distinction between them, be it in quantitative or qualitative terms. In this context, Sahni et al. [121] introduced a statefinder diagnostic method designed to differentiate among various DE models. This method relies on a pair of geometrical parameters known as statefinder parameters (r, s), which are defined as [121,122],

$$r = \frac{\dddot{a}}{aH^3}, \quad s = \frac{r-1}{3\left(q-\frac{1}{2}\right)}. \tag{23}$$

Within the framework of the linear redshift parametrization of $q(z)$, the formulations for the statefinder parameters (r, s) are presented as,

$$r(z) = (\alpha z+\beta)(2\alpha z+2\beta+1) + \alpha(1+z), \tag{24}$$

$$s(z) = \frac{2}{3}\left[\frac{\alpha(z+1)}{2\alpha z+2\beta-1} + \alpha z + \beta + 1\right]. \tag{25}$$

The statefinder parameters (r, s) play a crucial role in characterizing diverse DE models. Specifically, distinct values of (r, s) correspond to different DE scenarios: $r = 1, s = 0$ characterizes the ΛCDM model, while $r > 1, s < 0$ aligns with the Chaplygin gas model, and $r < 1, s > 0$ corresponds to the quintessence model. In Fig. 6, the evolution trajectories of the linear redshift parametrization model within the quintessence region ($r < 1, s > 0$) are illustrated for all constrained values of the model parameters. Intriguingly, these trajectories are anticipated to intersect the ΛCDM fixed point in the distant future.

3.4. $Om(z)$ Diagnostic

The $Om(z)$ diagnostic is a recently introduced method designed to effectively discriminate between various DE models [123]. Unlike the statefinder analysis, this method is notably simpler, providing a formula

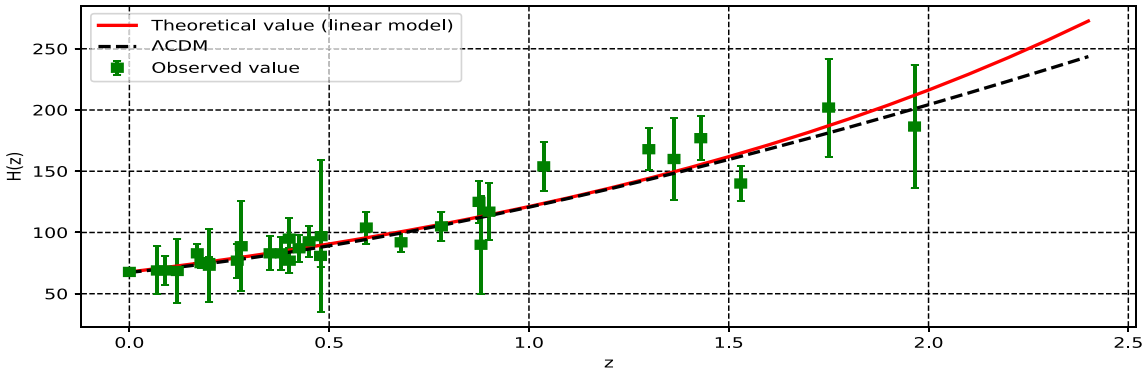

Fig. 1. The plot displays error bars for $H(z)$ against z comparing the linear redshift parametrization model (depicted by the red curve) with the ΛCDM model (represented by the black dotted curve). The individual data points from the $H(z)$ dataset are illustrated as green dots, providing a visual comparison between the theoretical predictions of the two models and the empirical observations across different redshifts. (For interpretation of the references to color in this figure legend, the reader is referred to the web version of this article.)

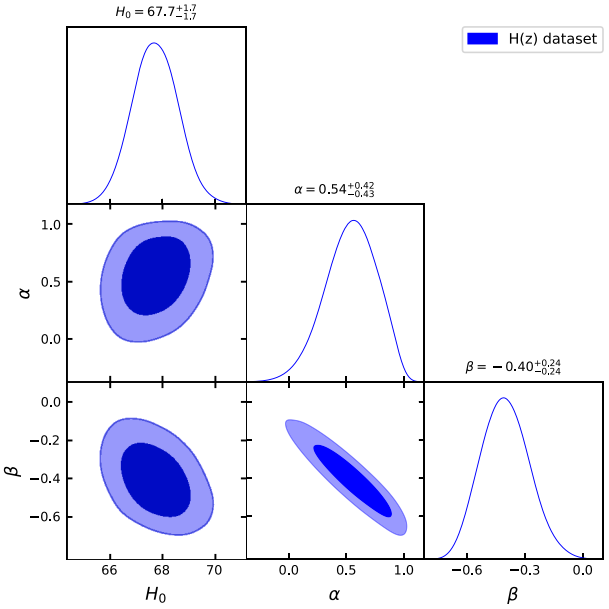

Fig. 2. The 1-σ and 2-σ confidence intervals for the parameters related to the $H(z)$ dataset.

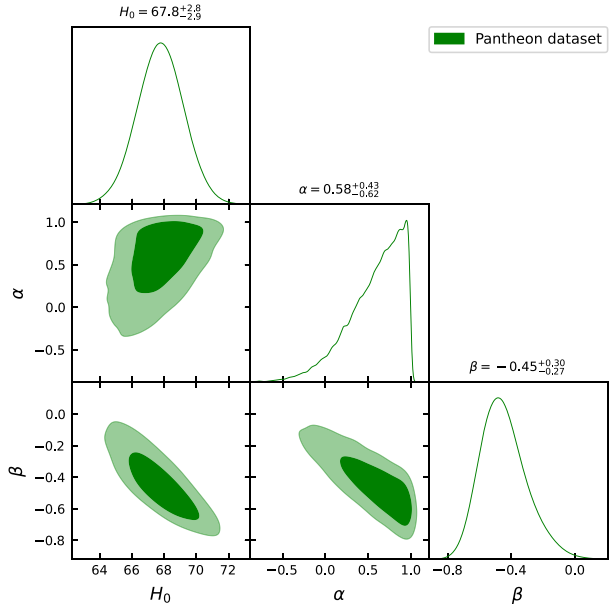

Fig. 3. The 1-σ and 2-σ confidence intervals for the parameters related to the *Pantheon* dataset.

that involves solely the Hubble parameter. Under the spatially flat constraint, the formula is expressed as,

$$Om(z) = \frac{\left(\frac{H(z)}{H_0}\right)^2 - 1}{(1+z)^3 - 1}. \tag{26}$$

Within the framework of the linear redshift parametrization of $q(z)$, the $Om(z)$ diagnostic is expressed as,

$$Om(z) = \frac{e^{2\alpha z}(1+z)^{-2\alpha+2\beta+2} - 1}{(1+z)^3 - 1} \tag{27}$$

A negative slope observed in $Om(z)$ signifies quintessence behavior, while a positive slope indicates phantom behavior. The constancy of $Om(z)$ aligns with the ΛCDM-type behavior for the model. As depicted in Fig. 7, the $Om(z)$ diagnostic exhibits a negative slope in the present, suggesting that the linear redshift parametrization model adheres to the quintessence scenario according to the $Om(z)$ diagnostic test.

4. Physical parameters of the model

In this section, we examine the characteristics of energy density, pressure, EoS parameters, and energy conditions for the constrained values of the model parameters. Since the model parameter n does not directly influence the Hubble parameter expression in Eq. (16), we opted to set it to specific values to analyze the behavior of cosmological parameters. Jaybhaye et al. [76] investigated cosmological implications within the framework of $f(R, L_m)$ gravity. Their study examined the universe's dynamics using the specific model $f(R, L_m) = \frac{R}{2} + L_m^n$ and its effects on various cosmological parameters. In their analysis using the same data as ours, they obtained the following constraints: $n = 1.078^{+0.012}_{-0.013}$ for the $H(z)$ dataset, $n = 1.1472^{+0.0028}_{-0.00042}$ for the *Pantheon* dataset, and $n = 1.07 \pm 0.10$ for the $H(z) + Pantheon$ dataset.

4.1. Energy density, pressure, and EoS parameter

Using Eqs. (16), (12), and (13), we have generated plots illustrating the evolution of the energy density and pressure, depicted in Figs. 8 and 9, respectively. Notably, the energy density demonstrates the expected positive behavior and diminishes as the universe expands, eventually approaching zero in the distant future (i.e. $\rho \to 0$ at $z \to -1$). Conversely, the pressure exhibits positive behavior in the early universe ($z \gg 1$), influenced by the dominance of matter, and transitions to negative behavior in both the present and future. This shift suggests a

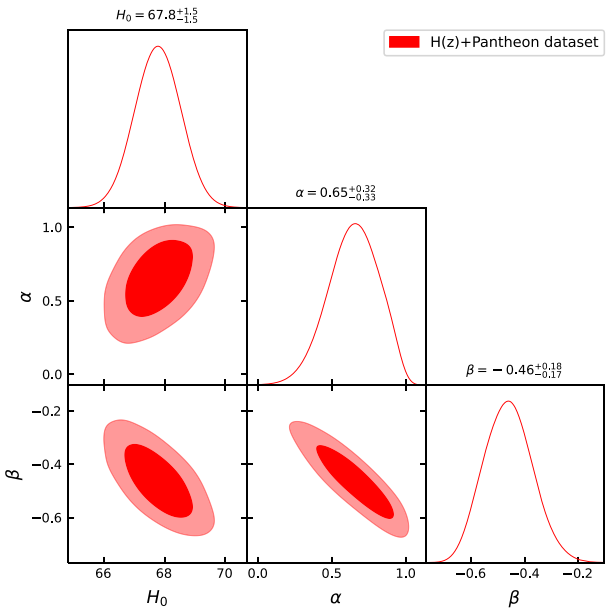

Fig. 4. The 1-σ and 2-σ confidence intervals for the parameters related to the $H(z) + Pantheon$ dataset.

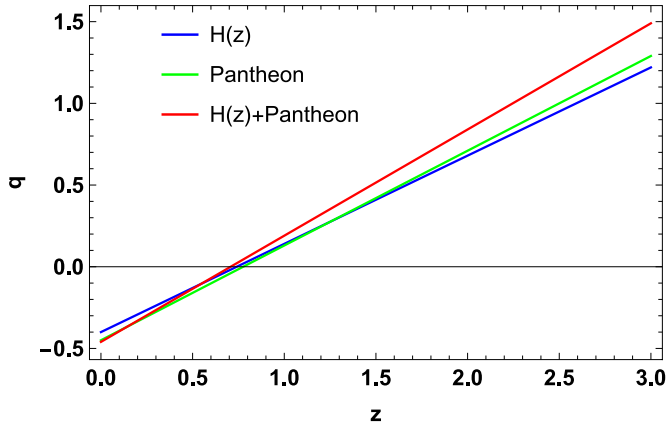

Fig. 5. The graph displays the relationship between the deceleration parameter q and redshift z.

driving force behind the universe's expansion. This finding supports the notion that the linear redshift parametrization of $q(z)$, when supported by additional terms in the $f(R, L_m)$ gravity model, contributes to the accelerated expansion of the universe.

The equation of state (EoS) parameter is expressed with the energy density and pressure as $\omega = \frac{p}{\rho}$. Here, ρ and p represent the density and pressure, respectively, encompassing all forms of matter (including both ordinary or baryonic matter and dark matter) as well as DE present in the universe. Using Eqs. (12) and (13), we can express the EoS parameter as:

$$\omega = -1 + \frac{(2 - 4\alpha)\dot{H}}{3\alpha H^2}. \tag{28}$$

Now, by employing the linear redshift parametrization of $q(z)$, the EoS parameter is given by

$$\omega(z) = -1 + \frac{2(2n - 1)(\alpha z + \beta + 1)}{3n}. \tag{29}$$

The EoS parameter is a crucial indicator used to categorize different phases of the universe's expansion, distinguishing between decelerated and accelerated periods [118]. In the matter-dominated phase, the EoS

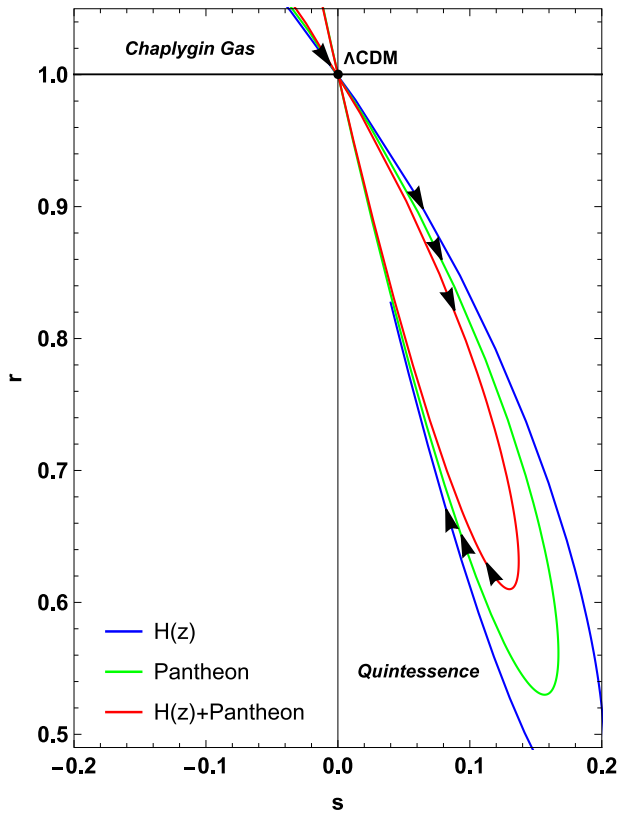

Fig. 6. The graph displays the evolutionary trajectories of the provided model in the $r - s$ plane.

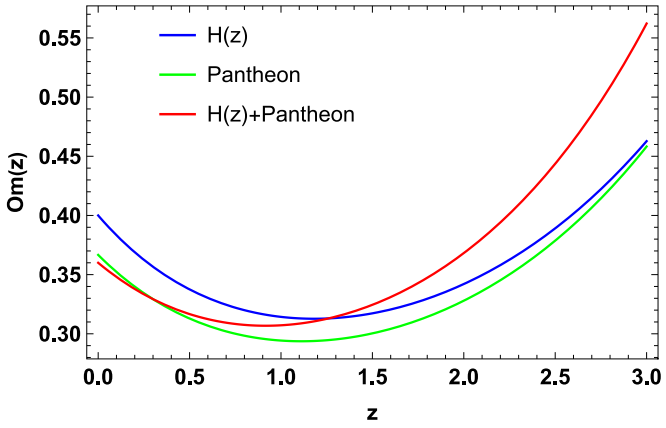

Fig. 7. The graph displays the relationship between the $Om(z)$ diagnostic and redshift z.

parameter is represented by $\omega = 0$. During the current accelerated phase of evolution, $-1 < \omega < -\frac{1}{3}$ corresponds to the quintessence phase, $\omega = -1$ represents the cosmological constant (ΛCDM) model, and $\omega < -1$ signifies the phantom phase. These distinctions are fundamental in characterizing the diverse dynamics and energy content of the universe at various stages of its evolution. The current value of the EoS parameter is determined and presented in Table 1. These results for ω_0 are consistent with the findings of various observational studies [124–127]. Furthermore, the EoS parameter's behavior, as depicted in Fig. 10, aligns with three distinct stages of the universe's evolution: radiation, matter, and DE eras. At high redshift values, $\omega = \frac{1}{3}$, corresponding to the EoS parameter during the primordial universe stage dominated by radiation. During this phase, the universe's dynamics were primarily

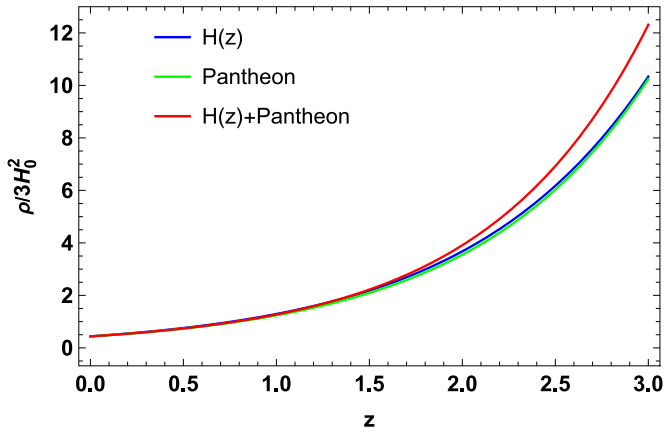

Fig. 8. The graph displays the relationship between the energy density ρ and redshift z.

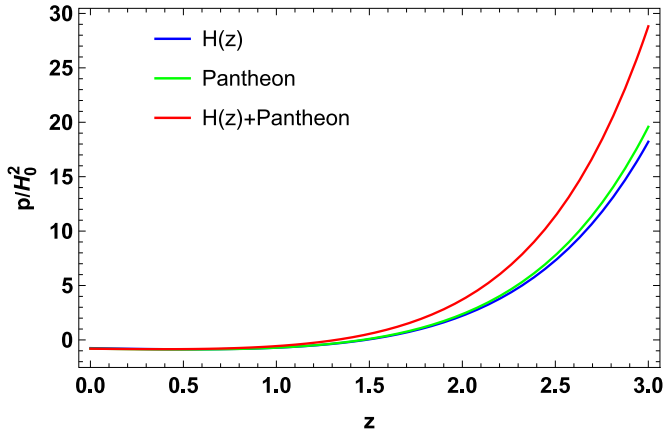

Fig. 9. The graph displays the relationship between the pressure p and redshift z.

influenced by radiation, which hindered the formation of the first atoms due to its high temperature [86]. As the universe cooled, atoms formed, leading to the subsequent creation of stars, galaxies, and galaxy clusters. This later stage, characterized by matter or pressureless matter, is indicated by $\omega = 0$ [86]. Fig. 10 illustrates that after the radiation-dominated period, ω indeed transitions through 0, signifying the matter-dominated phase of the universe's expansion. For lower redshift values, $-1 < \omega < -\frac{1}{3}$, confirming the quintessence nature of the universe's accelerated expansion phase, as discussed in Section 3 while examining the geometrical parameters. This observation supports the role of quintessence in driving the universe's current acceleration. In the standard model, the cosmological constant drives the universe into a DE-dominated phase, where a negative pressure fluid accelerates its expansion. However, in this approach, the linear redshift parametrization of $q(z)$ with additional terms in $f(R, L_m)$ is responsible for this significant feature, which notably circumvents the cosmological constant problem [128].

4.2. Energy conditions

In our current study, we will evaluate the viability of the linear redshift parametrization of $q(z)$ associated with the assumed $f(R, L_m)$ model by examining the energy conditions (ECs). The ECs serve as criteria imposed on the energy–momentum tensor to ensure the positivity of energy. These ECs are derived from Raychaudhuri's equation, which is a fundamental aspect of our analysis [129–131]. Specifically, these ECs are formulated as:

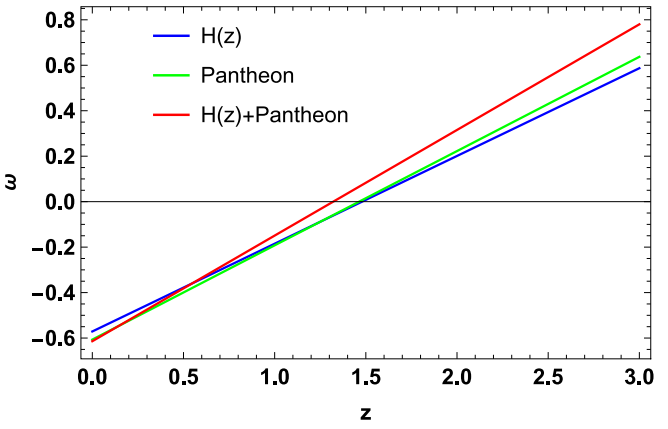

Fig. 10. The graph displays the relationship between the EoS parameter ω and redshift z.

- Null energy condition (NEC): $\rho_{eff} + p_{eff} \geq 0$;
- Weak energy conditions (WEC): $\rho_{eff} \geq 0$ and $\rho_{eff} + p_{eff} \geq 0$;
- Dominant energy conditions (DEC): $\rho_{eff} \geq 0$ and $|p_{eff}| \leq \rho_{eff}$.
- Strong energy conditions (SEC): $\rho_{eff} + 3p_{eff} \geq 0$.

Here, ρ_{eff} denotes the effective energy density, while p_{eff} represents the effective pressure. Below are the figures illustrating the evolution of ECs. The primary objective of these ECs is to assess the expansion of the universe. They manifest in various forms, including the NEC, WEC, DEC, and SEC. The violation of the NEC indicates that none of the aforementioned ECs are satisfied. The violation of the SEC is currently a subject of significant interest due to the observed accelerated expansion of the universe [132,133]. According to cosmological scenarios, the SEC must be violated during the inflationary expansion and at the present time [134]. From Figs. 11 and 12, it is evident that the NEC and DEC satisfy the positivity requirements throughout the entire range of redshifts, corresponding to the model parameters obtained from the observational datasets. Since the WEC is composed of energy density and NEC, it is also satisfied. Finally, from Fig. 13, we observe a violation of the SEC, indicating that the combination of energy density and pressure leads to a negative value. This violation is a characteristic feature of dark energy models, where the presence of a negative pressure component is responsible for the accelerated expansion of the universe. While the violation of the SEC may seem counterintuitive, it is consistent with the observed accelerated expansion and is a key aspect of our model's ability to explain cosmological dynamics beyond standard general relativity.

5. Conclusion

The present situation of the universe's accelerated expansion has become increasingly intriguing with time, prompting extensive research into various dynamical DE models and modified gravity theories. These models and theories have been employed in diverse ways to seek a suitable description of the accelerating universe. As observational data continues to improve in quality and quantity, the quest to understand the nature of DE and the dynamics of cosmic acceleration remains a central focus of modern cosmology. The exploration of alternative theories, such as $f(R, L_m)$ gravity, provides valuable potential avenues for addressing the challenges posed by the observed accelerated expansion, offering new perspectives on the fundamental laws governing the cosmos.

In this paper, we delved into the universe's accelerated expansion, focusing on the linear redshift parametrization of $q(z)$ in the context of $f(R, L_m)$ gravity, where R represents the Ricci scalar and L_m stands

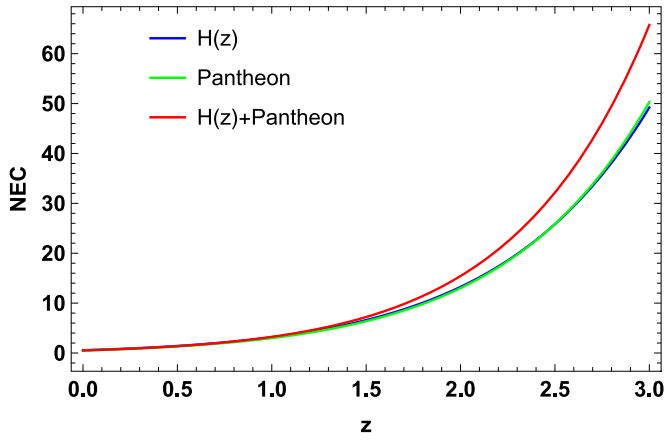

Fig. 11. The graph displays the relationship between the NEC and redshift z.

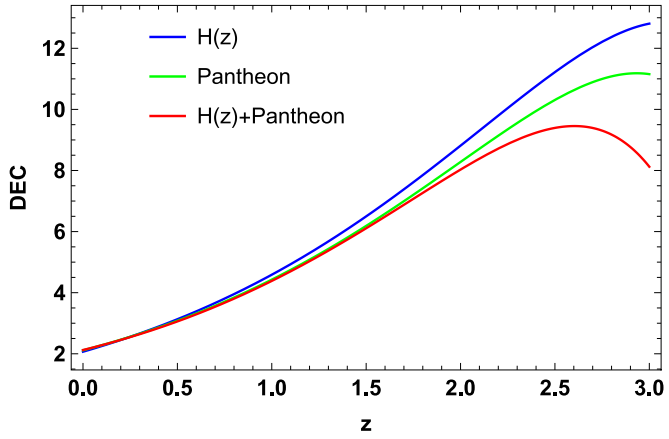

Fig. 12. The graph displays the relationship between the DEC and redshift z.

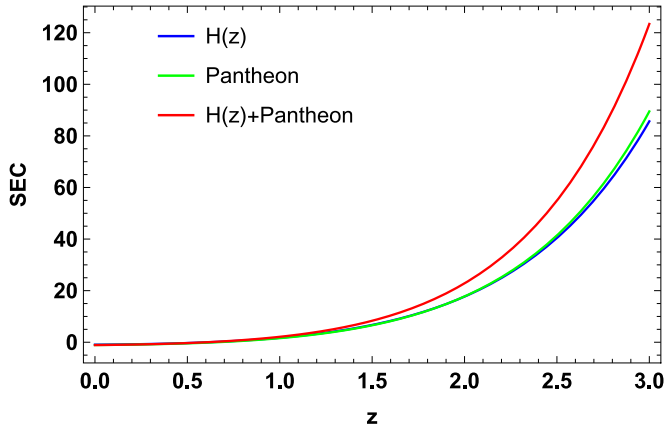

Fig. 13. The graph displays the relationship between the SEC and redshift z.

for the matter Lagrangian. Our investigation centered on the nonlinear functional form of $f(R, L_m)$ given by $f(R, L_m) = R/2 + L_m^n$, with n as a free parameter in the model. In addition, we explored the parametrization form of the deceleration parameter $q(z) = \alpha z + \beta$, where α and β are the model parameters [80]. By employing this parametrization, we derived the solution for the Hubble parameter as $H(z) = H_0 e^{\alpha z}(1+z)^{-\alpha+\beta+1}$. Moreover, we determined the best-fit values for the model parameters using the $H(z)$ dataset, the recently published *Pantheon* dataset, and their combined $H(z)$ + *Pantheon* dataset. The resulting best-fit values are as follows: for the $H(z)$ dataset, $H_0 = 67.7^{+1.7}_{-1.7}$, $\alpha = 0.54^{+0.42}_{-0.43}$ and $\beta = -0.40^{+0.24}_{-0.24}$; for the *Pantheon* dataset, $H_0 = 67.8^{+2.8}_{-2.9}$, $\alpha = 0.58^{+0.43}_{-0.62}$ and $\beta = -0.45^{+0.30}_{-0.27}$; and for the combined $H(z)+Pantheon$ dataset, $H_0 = 67.8^{+1.5}_{-1.5}$, $\alpha = 0.65^{+0.33}_{-0.32}$ and $\beta = -0.46^{+0.18}_{-0.17}$. Here, the current value of the deceleration parameter $q_0(z = 0) = \beta$ indicates that the universe is currently undergoing accelerated expansion. We analyzed the behavior of several cosmological parameters, as functions of the redshift z. These analyses are depicted in Figs. 5–13, corresponding to the best-fit values of the model parameters. Fig. 5 indicates a recent transition of the universe from a decelerated to an accelerated phase. Moreover, the evolution of the statefinder, $Om(z)$ diagnostics, and EoS parameter in Figs. 6, 7, and 10 suggest the quintessence nature of the universe's accelerating expansion phase. In our model, we have calculated the EoS parameter $\omega(z)$ and found that it lies in the range $-1 < \omega < -\frac{1}{3}$ during the present epoch. This range is characteristic of quintessence, which is a form of dark energy with a dynamic scalar field driving the acceleration, as opposed to a cosmological constant with $\omega = -1$. Zhadyranova et al. [23] investigated the late-time cosmic acceleration within the framework of a linear $f(T)$ cosmological model. Their analysis incorporates constraints from various datasets, including SNe Ia, Hubble data, and BAO. They found that the EoS parameter exhibits behavior similar to quintessence, with its present value being $\omega_0 = -0.68$. In Fig. 8, the energy density exhibits the expected positive behavior, while Fig. 9 shows that the isotropic pressure displays negative behavior, indicating a potential driver for the universe's accelerating expansion. Finally, the energy conditions presented in Figs. 11–13 show positive behavior for the NEC and DEC, while indicating a violation for the SEC in the present and future, supporting the observed acceleration.

While our model demonstrates compatibility with observational data, there are several avenues for future research that could further enhance our understanding of cosmology. Exploring alternative functional forms of $f(R, L_m)$ gravity, such as exponential or logarithmic forms, could provide a deeper understanding of the behavior of dark energy and the dynamics of cosmic expansion. Incorporating additional observational constraints, such as those from LSS surveys, CMB experiments, or future gravitational wave detections, would improve the accuracy of our cosmological models and test them against a wider range of observational data. Extending the analysis to more complex cosmological scenarios, such as inhomogeneous or anisotropic universes, could provide a more comprehensive understanding of gravitational theories beyond standard general relativity. In addition, investigating the impact of modified gravity on early universe cosmology, such as inflationary scenarios or the generation of primordial perturbations, could shed light on the fundamental physics governing the universe's earliest moments.

CRediT authorship contribution statement

Yerlan Myrzakulov: Writing – review & editing, Writing – original draft, Methodology, Investigation, Conceptualization. **O. Donmez:** Writing – review & editing, Writing – original draft, Conceptualization. **G. Dilara A. Yildiz:** Conceptualization, Data curation, Investigation, Methodology, Writing – original draft, Writing – review & editing. **E. Güdekli:** Conceptualization, Data curation, Investigation, Methodology, Writing – original draft, Writing – review & editing. **S. Muminov:** Conceptualization, Data curation, Investigation, Methodology, Writing – original draft, Writing – review & editing. **J. Rayimbaev:** Writing – review & editing, Writing – original draft.

Declaration of competing interest

The authors declare that they have no known competing financial interests or personal relationships that could have appeared to influence the work reported in this paper.

Data availability

No data was used for the research described in the article.

Acknowledgments

This research was funded by the Science Committee of the Ministry of Science and Higher Education of the Republic of Kazakhstan (Grant No. AP22682760).

References

[1] B.P. Abbott, Phys. Rev. Lett. 116 (2016) 061102.
[2] B.P. Abbott, et al., Phys. Rev. Lett. 116 (2016) 241103.
[3] B.P. Abbott, Phys. Rev. Lett. 118 (2017) 221101.
[4] B.P. Abbott, Phys. Rev. Lett. 119 (2017) 141101.
[5] B.P. Abbott, et al., Phys. Rev. Lett. 119 (2017) 161101.
[6] V. Sahni, A. Starobinsky, Internat. J. Modern Phys. D 9 (2000) 373.
[7] S.M. Carroll, Living Rev. Relat. 4 (2001) 1.
[8] P.J.E. Peebles, B. Ratra, Rev. Mod. Phys. 75 (2003) 559.
[9] T. Padmanabhan, Phys. Rep. 380 (2003) 235.
[10] S. Nojiri, S.D. Odintsov, Int. J. Geom. Methods Mod. Phys. 4 (2007) 115.
[11] W. Hu, I. Sawicki, Phys. Rev. D 76 (2007) 064004.
[12] S.A. Appleby, R.A. Battye, Phys. Lett. B 654 (2007) 7.
[13] A.A. Starobinsky, JETP Lett. 86 (2007) 157.
[14] T. Harko, et al., Phys. Dark Univ. 34 (2021) 100886.
[15] N. Myrzakulov, R. Myrzakulov, L. Ravera, Symmetry 13 (2021) 1855.
[16] D. Iosifidis, N. Myrzakulov, R. Myrzakulov, Universe 7 (2021) 262.
[17] M. Koussour, et al., Fortschr. Phys. 71 (2023) 2200172.
[18] M. Koussour, et al., Nuclear Phys. B 990 (2023) 116158.
[19] M. Koussour, et al., Phys. Dark Univ. 36 (2022) 101051.
[20] M. Koussour, et al., J. High Energy Phys. 37 (2023) 15–24.
[21] M. Koussour, M. Bennai, Chinese J. Phys. 79 (2022) 339–347.
[22] M. Koussour, et al., Phys. Dark Univ. 45 (2024) 101527.
[23] A. Zhadyranova, et al., Phys. Dark Univ. 45 (2024) 101514.
[24] A. Zhadyranova, M. Koussour, S. Bekkhozhayev, Chinese J. Phys. 89 (2024) 1483–1492.
[25] I. Zlatev, L. Wang, P.J. Steinhardt, Phys. Rev. Lett. 82 (1999) 896.
[26] M.S. Turner, Internat. J. Modern Phys. A 17 (2002) 180.
[27] V. Sahni, Class. Quantum Gravity 19 (2002) 3435.
[28] T. Chiba, T. Okabe, M. Yamaguchi, Phys. Rev. D 62 (2000) 023511.
[29] M.R. Setare, Eur. Phys. J. C 52 (2007) 689.
[30] A.E. Bernardini, O. Bertolami, Phys. Rev. D 77 (2008) 083506.
[31] S.D.H. Hsu, Phys. Lett. B 594 (2004) 13.
[32] M. Li, Phys. Lett. B 603 (2004) 1.
[33] K. Bamba, Astrophys. Space Sci. 342 (2012) 155228.
[34] A.G. Riess, et al., Astron. J. 116 (1998) 1009.
[35] S. Perlmutter, et al., Astrophys. J. 517 (1999) 565.
[36] C.L. Bennett, et al., Astrophys. J. Suppl. 148 (2003) 119–134.
[37] R.R. Caldwell, M. Doran, Phys. Rev. D 69 (2004) 103517.
[38] D.N. Spergel, et al., WMAP Collaboration, Astrophys. J. Suppl. 148 (2003) 175.
[39] D.J. Eisenstein, et al., Astrophys. J. 633 (2005) 560.
[40] W.J. Percival, et al., Mon. Not. R. Astron. Soc. 401 (2010) 2148.
[41] T. Koivisto, D.F. Mota, Phys. Rev. D 73 (2006) 083502.
[42] S.F. Daniel, Phys. Rev. D 77 (2008) 103513.
[43] H.A. Buchdahl, Mon. Not. R. Astron. Soc. 150 (1970) 1.
[44] R. Kerner, Gen. Relativity Gravitation 14 (1982) 453.
[45] H. Kleinert, H.J. Schmidt, Gen. Relativity Gravitation 34 (2002) 1295.
[46] S.M. Carroll, et al., Phys. Rev. D 70 (2004) 043528.
[47] S. Capozziello, et al., Phys. Lett. B 639 (2006) 135.
[48] L. Amendola, D. Polarski, S. Tsujikawa, Phys. Rev. Lett. 98 (2007) 131302.
[49] S. Nojiri, S.D. Odintsov, Phys. Rev. D 68 (2003) 123512.
[50] V. Faraoni, Phys. Rev. D 74 (2006) 023529.
[51] P.J. Zhang, Phys. Rev. D 76 (2007) 024007.
[52] L. Amendola, S. Tsujikawa, Phys. Lett. B 660 (2008) 125.
[53] S. Tsujikawa, Phys. Rev. D 77 (2008) 023507.
[54] T. Liua, X. Zhanga, W. Zhaoa, Phys. Lett. B 777 (2018) 286–293.
[55] S. Capozziello, S. Tsujikawa, Phys. Rev. D 77 (2008) 107501.
[56] S.M. Carroll, et al., Phys. Rev. D 70 (2004) 043528.
[57] A.A. Starobinsky, JETP Lett. 86 (2007) 157–163.
[58] S. Nojiri, S.D. Odintsov, Phys. Lett. B 657 (2007) 238.
[59] S. Nojiri, S.D. Odintsov, Phys. Rev. D 77 (2008) 026007.
[60] G. Cognola, et al., Phys. Rev. D 77 (2008) 046009.
[61] J. Santos, et al., Phys. Rev. D 76 (2007) 083513.
[62] S. Capozziello, V.F. Cardone, V. Salzano, Phys. Rev. D 78 (2008) 063504.
[63] R.C. Nunes, et al., J. Cosmol. Astropart. 2017 (01) (2017) 005.
[64] O. Bertolami, et al., Phys. Rev. D 75 (2007) 104016.
[65] T. Harko, Phys. Lett. B 669 (2008) 376.
[66] T. Harko, Phys. Rev. D 81 (2010) 084050.
[67] T. Harko, Phys. Rev. D 81 (2010) 044021.
[68] S. Nesseris, Phys. Rev. D 79 (2009) 044015.
[69] V. Faraoni, Phys. Rev. D 76 (2007) 127501.
[70] V. Faraoni, Phys. Rev. D 80 (2009) 124040.
[71] T. Harko, F.S.N. Lobo, Eur. Phys. J. C 70 (2010) 373–379.
[72] V. Faraoni, Cosmology in Scalar-Tensor Gravity, Kluwer Academic, Dordrecht, 2004.
[73] O. Bertolami, J. Páramos, S. Turyshev, arXiv, arXiv:gr-qc/0602016.
[74] J. Wang, K. Liao, Classical Quantum Gravity 29 (2012) 215016.
[75] B.S. Goncalves, P.H.R.S. Moraes, Fortschr. Phys. 71 (2023) 2200153.
[76] L.V. Jaybhaye, et al., Phys. Lett. B 831 (2022) 137148.
[77] N. Myrzakulov, et al., Eur. Phys. J. Plus 138 (2023) 852.
[78] S. Myrzakulova, M. Koussour, N. Myrzakulov, Phys. Dark Univ. 43 (2024) 101399.
[79] M.S. Turner, A.G. Riess, Astrophys. J. 569 (2002) 18.
[80] A.G. Riess, et al., Astrophys. J. 607 (2004) 665.
[81] Y.G. Gong, A. Wang, Phys. Rev. D 75 (2007) 043520.
[82] J.V. Cunha, J.A.S. Lima, Mon. Not. R. Astron. Soc. 390 (2008) 210.
[83] R. Nair, et al., J. Cosmol. Astropart. Phys. 01 (2012) 018.
[84] O. Akarsu, et al., Eur. Phys. J. Plus 129 (2014) 22.
[85] A.A. Mamon, S. Das, Internat. J. Modern Phys. D 25 (2016) 1650032.
[86] B. Ryden, Introduction to Cosmology, Addison Wesley, San Francisco, United States of America, 2003.
[87] T. Harko, F.S.N. Lobo, Galaxies 2014 (2) (2014) 410–465.
[88] T. Harko, et al., Eur. Phys. J. C 75 (2015) 386.
[89] S.K.J. Pacif, Eur. Phys. J. Plus 135 (2020) 10.
[90] S.K.J. Pacif, R. Myrzakulov, S. Myrzakul, Int. J. Geom. Methods Mod. Phys. 14 (2017) 07.
[91] J. Weller, A. Albrecht, Phys. Rev. D 65 (2002) 103512.
[92] M.P. Hobson, A.H. Jaffe, A.R. Liddle, P. Mukherjee, D. Parkison (Eds.), Bayesian Methods in Cosmology, Cambridge University Press, Cambridge, England, 2009.
[93] D.F. Mackey, et al., Publ. Astron. Soc. Pac. 125 (2013) 306.
[94] R. Jimenez, Astrophys. J. 573 (2002) 37.
[95] C. Zhang, et al., Res. Astron. Astrophys. 14 (2014) 1221.
[96] R. Jimenez, et al., Astrophys. J. 593 (2003) 622.
[97] M. Moresco, et al., J. Cosmol. Astropart. Phys. 2016 (2016) 014-014.
[98] J. Simon, L. Verde, R. Jimenez, Phys. Rev. D 71 (2005) 123001.
[99] M. Moresco, et al., J. Cosmol. Astropart. Phys. 2012 (2012) 006-006.
[100] D. Stern, et al., J. Cosmol. Astropart. Phys. 2010 (2010) 008.
[101] M. Moresco, Mon. Not. R. Astron. Soc. Lett. 450 (2015) L16–L20.
[102] A. Gómez-Valent, L. Amendola, J. Cosmol. Astropart. Phys. 2018 (2018) 051.
[103] M. López-Corredoira, et al., Astron. Astrophys. 600 (2017) A91.
[104] M. López-Corredoira, A. Vazdekis, Astron. Astrophys. 614 (2018) A127.
[105] L. Verde, P. Protopapas, R. Jimenez, Phys. Dark Univ. 5 (2014) 307–314.
[106] D.M. Scolnic, et al., Astrophys. J. 859 (2018) 101.
[107] R. Kessler, D. Scolnic, Astrophys. J. 836 (2017) 56.
[108] N. Aghanim, et al., Astron. Astrophys. 641 (2020) A6.
[109] J.F. Jesus, et al., J. Cosmol. Astropart. Phys. 04 (2020) 053–070.
[110] J.R. Garza, et al., Eur. Phys. J. C 79 (2019) 890.
[111] A. Al Mamon, K. Bamba, Eur. Phys. J. C 78 (2018) 862.
[112] O. Farooq, et al., Astrophys. J. 835 (2017) 26–37.
[113] A. Hernandez-Almada, et al., Eur. Phys. J. C 79 (2019) 12.
[114] S. Basilakos, F. Bauera, J. Sola, J. Cosmol. Astropart. Phys. 01 (2012) 050–079.
[115] M. Koussour, et al., Results Phys. 55 (2023) 107166.
[116] M. Koussour, N. Myrzakulov, M.K.M. Ali, J. High Energy Astrophys. 42 (2024) 96–103.
[117] Y. Myrzakulov, et al., J. High Energy Astrophys. 42 (2024) 209–216.
[118] D. Wang, et al., Eur. Phys. J. C 83 (2023) 1–14.
[119] N. Myrzakulov, et al., Eur. Phys. J. Plus 138 (2023) 852.
[120] N. Myrzakulov, et al., Chin. Phys. C 47 (2023) 115107.
[121] V. Sahni, et al., J. Exp. Theor. Phys. Lett. 77 (2003) 201–206.
[122] U. alam, et al., Mon. Not. R. Astron. Soc. 344 (2003) 1057.
[123] V. Sahni, A. Shafieloo, A.A. Starobinsky, Phys. Rev. D 78 (2008) 103502.
[124] S. Arora, A. Parida, P.K. Sahoo, Eur. Phys. J. C 81 (2021) 1–7.
[125] M. Koussour, A. De, Eur. Phys. J. C 83 (2023) 400.
[126] A. Mukherjee, Mon. Not. R. Astron. Soc. 460 (2016) 273–282.
[127] A. Nàjera, A. Fajardo, Phys. Dark Univ. 34 (2021) 100889.
[128] S. Weinberg, Rev. Mod. Phys. 61 (1989) 1.
[129] A. Raychaudhuri, Phys. Rev. D 98 (1955) 1123.
[130] S. Nojiri, S.D. Odintsov, Int. J. Geom. Methods Mod. Phys. 04 (2007) 115.
[131] J. Ehlers, Internat. J. Modern Phys. D 15 (2006) 1573.
[132] C. Barcelo, M. Visser, Internat. J. Modern Phys. D 11 (2002) 1553.
[133] P.H.R.S. Moraes, P.K. Sahoo, Eur. Phys. J. C 77 (2017) 480.
[134] M. Visser, Phys. Rev. D 56 (1997) 7578.